ELSEVIER

Journal of Alloys and Compounds 446–447 (2007) 614–619

Journal of ALLOYS AND COMPOUNDS

www.elsevier.com/locate/jallcom

Structure and electrochemical properties of composite electrodes synthesized by mechanical milling Ni-free $TiMn_2$-based alloy with La-based alloys

Hailiang Chu [a,b], Yao Zhang [a,*], Lixian Sun [a,*], Shujun Qiu [a,b], Yanni Qi [a,b], Fen Xu [a,*], Huatang Yuan [c]

[a] *Materials and Thermochemistry Laboratory, Dalian Institute of Chemical Physics, Chinese Academy of Sciences, Dalian 116023, China*

[b] *Graduate School of the Chinese Academy of Sciences, Beijing 100049, China*

[c] *Institute of New Energy Material Chemistry, Nankai University, Tianjin 300071, China*

Received 27 September 2006; received in revised form 25 December 2006; accepted 31 December 2006
Available online 16 January 2007

Abstract

In the present study, hydrogen storage composite electrodes were prepared by mechanical milling the powder mixtures of Ni-free Laves phase alloy $Ti_{0.9}Zr_{0.2}Mn_{1.5}Cr_{0.3}V_{0.3}$ (AB_2) with $LaNi_{3.8}Mn_{0.3}Al_{0.4}Co_{0.5}$ (AB_5) and $La_{0.7}Mg_{0.25}Zr_{0.05}Ni_{2.975}Co_{0.525}$ ($AB_{3.5}$), respectively. X-ray diffraction (XRD) measurements found that the basic phase structure (hexagonal C14) was still maintained in $TiMn_2$-based alloy after short-time mechanical milling with additional La-based alloys. The fine particles of La-based alloy were found dispersing over the bulk particle of $TiMn_2$-based alloy by observations of scanning electron microscopy (SEM) with energy dispersive spectrometer (EDS). The electrochemical studies showed that the additional La-based alloys greatly improved the discharge capacity of the composite electrode. The maximum discharge capacity reached 310.4 mAh/g and 314.0 mAh/g for AB_2–10 wt.% AB_5 and AB_2–10 wt.% $AB_{3.5}$ electrodes, respectively, which was much higher than the maximum 48.6 mAh/g of original $Ti_{0.9}Zr_{0.2}Mn_{1.5}Cr_{0.3}V_{0.3}$ alloy electrode. Electrochemical impedance spectroscopy (EIS) and cyclic voltammetry (CV) measurements suggests that $AB_{3.5}$-type alloy as a surface-modifier is beneficial to the decrease of the charge-transfer reaction resistance. The mechanical milling with AB_5-type alloy was found improving the hydrogen diffusion in the bulk of the alloy from the results of anodic polarization measurement.

Keywords: Hydrogen storage alloy electrodes; AB_2-type Laves phase alloy; Surface modification; Electrochemical properties; Mechanical milling

1. Introduction

Among the hydrogen storage alloys that have been extensively investigated, Ti-based AB_2-type Laves phase hydrogen storage alloys are potential candidates for negative electrode materials in Ni-MH batteries due to their larger hydrogen absorption capacities at ambient temperature [1]. Up to date, many Ni-contained Ti-based alloys have been extensively investigated [2–5] since Ni element is essentially important in Ti-based alloy electrodes because of its catalytic effect for the electrodes during electrochemical reactions. For example, the theoretical capacity of some Ti-based Laves phase alloy electrodes was reported to be about 540 mAh/g [6] and it could be activated easily within several charge–discharge cycles. Nevertheless, Ni-free-type Ti-based Laves alloys are rarely investigated in electrochemical systems although they exhibit even more hydrogen storage capacity in solid–gas reactions.

In recent years, the mechanical milling treatment is regarded as an effective method in surface modification and improving some electrochemical properties of the hydrogen storage alloys such as discharge capacity, cyclic stability or kinetics [7–9], etc. For example, the previous studies showed that mechanical milling with the $LaNi_5$ alloy could improve the activation behavior of Mg_2Ni [10] and $Zr_{0.5}Ti_{0.5}V_{0.75}Ni_{1.25}$ [11] alloy electrodes and also increase the electrochemical discharge capacity of

* Corresponding authors. Tel.: +86 411 84379213; fax: +86 411 84379213.
E-mail addresses: zhangyao@dicp.ac.cn (Y. Zhang), lxsun@dicp.ac.cn (L. Sun), fenxu@dicp.ac.cn (F. Xu).

0925-8388/$ – see front matter © 2007 Elsevier B.V. All rights reserved.
doi:10.1016/j.jallcom.2006.12.145

Ti–V-based BCC phase alloy [8]. Therefore, the mechanical milling method can be applied in this study to improve the electrochemical properties of our designed Ni-free $TiMn_2$-based hydrogen storage alloy electrode.

Up to now, many studies showed that some of new series of R–Mg–Ni-based (where R is a rare earth or Y, Ca) alloys with higher hydrogen storage capacity were developed. Pan et al. [12,13] investigated La–Mg-based $La_{0.7}Mg_{0.3}(Ni_{0.85}Co_{0.15})_x$ ($x = 2.5$–5.0) alloys that consisted of $LaNi_5$ phase and $(LaMg)Ni_3$ phase, and revealed that the maximum electrochemical discharge capacity was 395.6 mAh/g, which was much higher than that of the commercially used $LaNi_5$-type alloys. Furthermore, its cyclic stability, activation properties and the high-rate dischargeability were superior to those of most Ti-based alloy electrodes. Therefore, it can be expected that the discharge capacity and electrochemical hydrogen reaction kinetics of our designed Ni-free $Ti_{0.9}Zr_{0.2}Mn_{1.5}Cr_{0.3}V_{0.3}$ alloy electrode could be improved by mechanical milling with this kind of La–Mg-based alloy.

As mentioned above, the structure of La–Mg-based alloy is different from that of AB_5-type alloy and its electrochemical properties are superior to those of AB_5-type alloy. Therefore, in this study, AB_5-type alloy $LaNi_{3.8}Mn_{0.3}Al_{0.4}Co_{0.5}$ and La–Mg-based $AB_{3.5}$-type alloy $La_{0.7}Mg_{0.25}Zr_{0.05}Ni_{2.975}Co_{0.525}$ were selected as surface modifiers for Ni-free Laves phase $Ti_{0.9}Zr_{0.2}Mn_{1.5}Cr_{0.3}V_{0.3}$ alloy. The AB_2–AB_5 and AB_2–$AB_{3.5}$ composites were prepared by mechanical milling method. Their structures and respective effects on the electrochemical performances were investigated systematically in the present work.

2. Experimental

Nonstoichiometric Ni-free AB_2-type Laves phase alloy $Ti_{0.9}Zr_{0.2}Mn_{1.5}Cr_{0.3}V_{0.3}$, AB_5-type alloy $LaNi_{3.8}Mn_{0.3}Al_{0.4}Co_{0.5}$ and $AB_{3.5}$-type alloy $La_{0.7}Mg_{0.25}Zr_{0.05}Ni_{2.975}Co_{0.525}$ were prepared by vacuum magnetic levitation melting under argon atmosphere. The ingots were turned over and re-melted three times for homogeneity. The purity of starting elemental metals was higher than 99%. Then the ingots were mechanically crushed and ground into the powder of 200-mesh size for mechanical milling treatment. These alloys were represented as AB_2 alloy, AB_5 alloy and $AB_{3.5}$ alloy hereafter, respectively.

The alloy powder of AB_2 was mixed homogenously in the weight ratio of 9.0:1.0 with AB_5 and $AB_{3.5}$ alloy powder, respectively, and ground by QM-1SP planetary ball miller under 0.2–0.3 MPa argon atmosphere for 2 h. In each stainless milling pot, the ball-to-powder weight ratio was 20:1. As compared, the AB_2 alloy was ball milled under the same condition. The crystal structure of the alloys was characterized by XRD (Rigaku D/max-2500, Cu Kα, 40 kV, 250 mA). The surface morphologies of the alloys were observed using scanning electron microscopy (SEM, JSM6360LV) linked with energy dispersive X-ray spectrometer (EDS, Oxford INCA). A N4 plus laser scattering particle meter was used to measure particle size distribution of alloy powder.

The tested electrodes for electrochemical measurements were fabricated by mixing 100 mg the prepared alloy powder with 300 mg electrolytic Ni powder. The mixture was then pressed into a pellet of 10 mm in diameter under a pressure of 30 MPa. Both sides of the electrode pellet were coated with two foam nickel sheets, then pressed at 6 MPa and tightly spot-welded. A nickel lead wire was attached to this pressed foam nickel sheet by spot welding. Electrochemical measurements were performed at 303 K in a standard open tri-electrode electrolysis cell consisting of a working electrode (the MH pellet electrode for studying), a sintered $Ni(OH)_2$/NiOOH counter electrode, and a Hg/HgO reference electrode immersed in the 6 M KOH electrolyte. Charge–discharge cycles of alloy electrodes were conducted by an automatic LAND battery test instrument. The electrodes were charged for 2 h at a current density of 300 mA/g, rested for 5 min and then discharged to the cut-off potential of −0.6 V versus Hg/HgO reference electrode at a current density of 100 mA/g.

The electrochemical impedance spectroscopy (EIS), cyclic voltammograms (CV) and anodic polarization (AP) measurements were conducted on Zahner Elektrik IM6e electrochemical workstation at 50% depth of discharge (DOD) at 303 K. The scan rate of CV measurements was 50 mV/s within the scan potential range from −1.2 V to 0 V. The frequency range of EIS was from 10 kHz to 5 mHz with an amplitude of 5 mV versus open circuit potential. Before the EIS and CV measurements, the alloy electrodes were first activated by charge–discharge for three cycles. The anodic polarization curves were measured by scanning the electrode potential with the rate of 5 mV/s from 0 mV to 600 mV (versus open circuit potential). The hydrogen diffusion coefficient was determined by potential step method, which was performed under the constant potential of +500 mV for 3600 s at the fully charged state of the fourth charge–discharge cycle.

3. Results and discussion

3.1. The microstructure and morphology

Fig. 1 shows that X-ray diffraction patterns of ball-milled AB_2 alloy, AB_2–AB_5 and AB_2–$AB_{3.5}$ composite alloys. It was found that the Ti–Mn-based AB_2 alloy could be indexed as the hexagonal C14 Laves phase and some impurity of metallic vanadium. It was also found that mechanical milling with 10 wt.% rare-earth alloys did not change the basic structure (hexagonal C14 Laves phase) of the original AB_2 alloy. Fig. 2 illustrates that SEM images and EDS patterns of ball-milled AB_2 alloy and AB_2–$AB_{3.5}$ composites. It was found that both AB_2 alloy particles and rare-earth alloy particles were reduced in size. The surface of the milled alloy particles became much rougher after mechanical milling. This means that some fresh surfaces have been generated during the process of mechanical milling. In the case of ball-milled AB_2–10 wt.% $AB_{3.5}$ composite alloy, as seen from Fig. 2(b), the differences of EDS patterns between micro-area (I) and (II) revealed that the small and white particles on the surface of the bulk alloy were the $La_{0.7}Mg_{0.25}Zr_{0.05}Ni_{2.975}Co_{0.525}$ alloy particles which adhered to the bulk of $Ti_{0.9}Zr_{0.2}Mn_{1.5}Cr_{0.3}V_{0.3}$ alloy particles. This phenomenon resulted from the different hardness and ductility

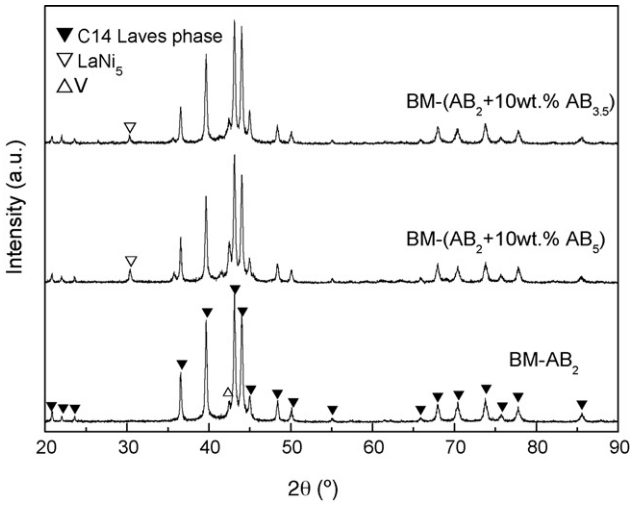

Fig. 1. The XRD patterns of ball-milled AB_2 alloy and AB_2–10 wt.% AB_5, AB_2–10 wt.% $AB_{3.5}$ composites.

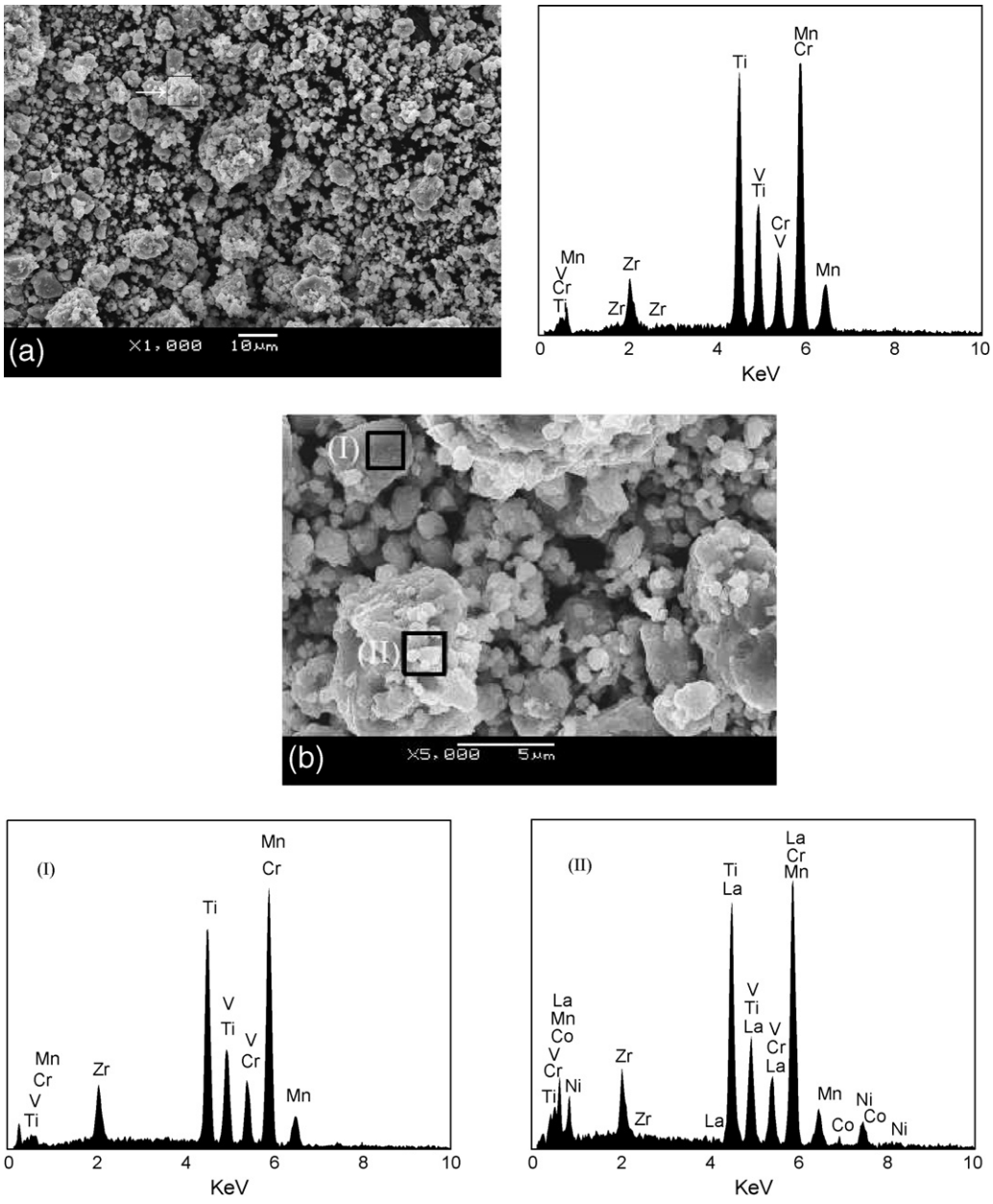

Fig. 2. SEM images and EDS patterns of composites: (a) ball-milled AB_2; (b) ball-milled AB_2–10 wt.% $AB_{3.5}$.

between the two alloys. The rare-earth alloy particles might be pulverized more easily and adhered to the surface of the larger $Ti_{0.9}Zr_{0.2}Mn_{1.5}Cr_{0.3}V_{0.3}$ alloy particles according to the detection of EDS.

3.2. The dischargeability of the composite electrodes

Fig. 3 presents the discharge curves of ball-milled AB_2, AB_2–AB_5 and AB_2–$AB_{3.5}$ alloy electrodes at the largest discharge capacity and some electrochemical properties are summarized in Table 1. As seen from Fig. 3, a discharge capacity of 48.6 mAh/g without an apparent discharge plateau was observed for ball-milled AB_2 alloy electrode, which was ascribed to the absence of Ni element that had a catalytic effect on the charge transfer reaction [14] in the AB_2 alloy. However, as concerns to AB_2–AB_5 and AB_2–$AB_{3.5}$ composite alloys, the discharge capacity had been greatly improved, which reached 310.4 mAh/g and 314.0 mAh/g, respectively. Furthermore, it was found that a flatter discharge plateau was observed at the potential of about −0.90 V for each discharge curve. The appreciable increase of the discharge capacity is ascribed to

Table 1
The electrochemical properties of the ball-milled AB_2, AB_2–AB_5 and AB_2–$AB_{3.5}$ composite electrodes

Samples	N_a[a]	C_{max} (mAh/g)	C_{20} (mAh/g)	C_{20}/C_{max} (%)
BM-AB_2	1	48.6	28.9	59.5
BM-(AB_2–AB_5)	2	310.4	113.2	36.5
BM-(AB_2–$AB_{3.5}$)	2	314.0	123.8	39.4

[a] The cycle numbers needed to activate the composite electrodes.

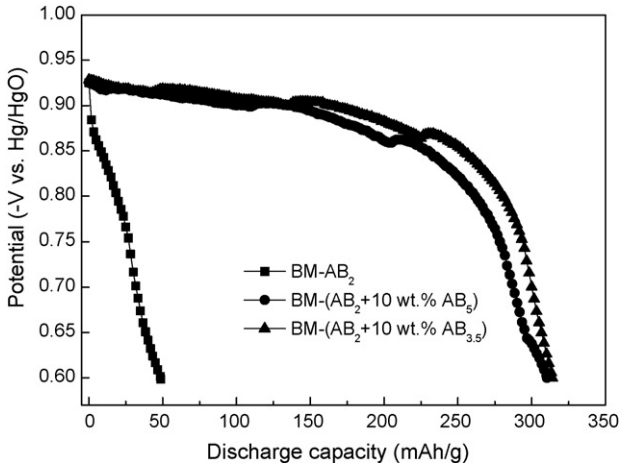

Fig. 3. Discharge potential curves of ball-milled AB_2, AB_2–AB_5 and AB_2–$AB_{3.5}$ composite electrodes at the largest discharge capacity at 303 K.

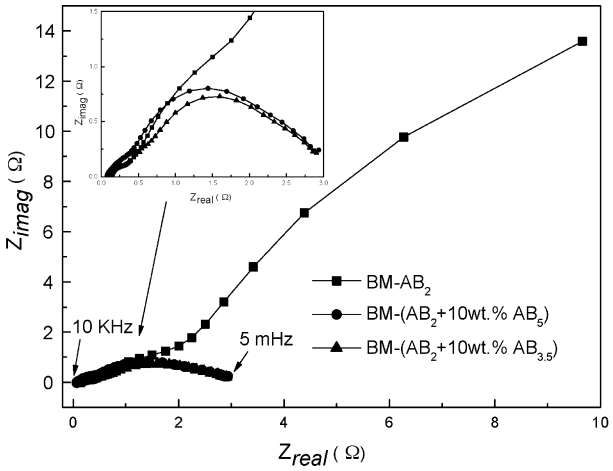

Fig. 5. Electrochemical impedance spectra (EIS) of ball-milled AB_2, AB_2–AB_5 and AB_2–$AB_{3.5}$ composite electrodes at 50% DOD at 303 K.

the incorporated rare-earth alloy particles on the surface layer of the ball-milled AB_2–AB_5 and AB_2–$AB_{3.5}$ composite samples. It can be suggested that the La-based alloy particles not only act as an electro-catalyst and a micro-current collector on the surface for hydrogen evolution reaction, but also provide hydrogen diffusion pathways during electrochemical reaction. This is beneficial to the improvement of reaction kinetics and charge–discharge capacity of the composite electrodes. Fig. 4 illustrates the discharge capacity versus cycle number of the ball-milled AB_2, AB_2–AB_5 and AB_2–$AB_{3.5}$ alloy electrodes. We noticed that, although the ball-milled AB_2 alloy electrode had an improved cycling stability (see Table 1), it still could not meet the requirements of practical application due to its lower discharge capacity. For ball-milled AB_2–AB_5 and AB_2–$AB_{3.5}$ composite electrodes, it needs only two charge–discharge cycles (see Table 1) to be fully activated. However, the discharge capacity rapidly decreased to 113.2 mAh/g and 123.8 mAh/g after 20 charge–discharge cycles for AB_2–AB_5 and AB_2–$AB_{3.5}$ composites, respectively. Further investigations on improving the cycling stability of the alloy electrodes are underway in our laboratory.

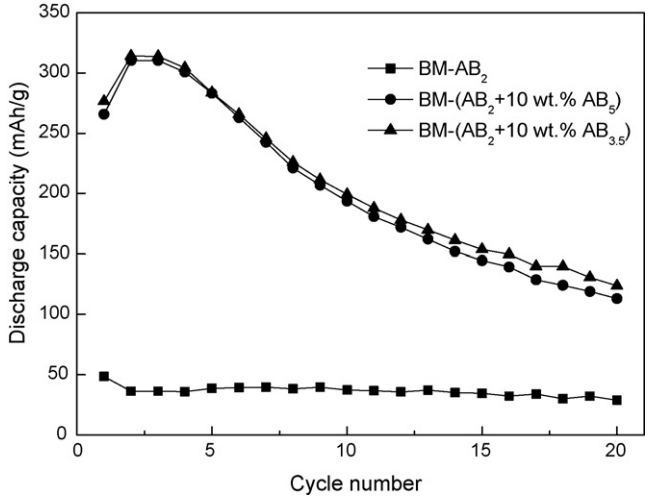

Fig. 4. Discharge capacity as a function of cycle number of ball-milled AB_2, AB_2–AB_5 and AB_2–$AB_{3.5}$ composite electrodes at 303 K.

3.3. The reaction kinetics of the composite electrodes

Fig. 5 illustrates the electrochemical impedance spectra of ball-milled AB_2, AB_2–AB_5 and AB_2–$AB_{3.5}$ alloy electrodes at 50% DOD at 303 K. It was found that all the EIS spectra of these alloy electrodes consisted of a small semicircle in the high-frequency region and a large semicircle in the low-frequency region. Kuriyama et al. [15] explained that the large semicircle in the low-frequency region was attributed to the chare-transfer reaction resistance at the electrode surface. As shown in Fig. 5, the radius of large semicircle in the low-frequency region of ball-milled AB_2 alloy electrode was greatly larger than that of AB_2–AB_5 and AB_2–$AB_{3.5}$ composite alloy electrodes, which indicated that the charge-transfer resistance decreased to a great extent after mechanical milling AB_2 alloy with rare-earth alloys AB_5 and $AB_{3.5}$, respectively. Thus, it was believed that the rare-earth alloys AB_5 and $AB_{3.5}$ played an important role in improving the hydrogen reaction kinetics, especially in decreasing the charge-transfer resistance on the surface of alloy electrodes. Furthermore, the radius of large semicircle in the low-frequency region of AB_2–$AB_{3.5}$ composite alloy electrode was smaller than that of AB_2–AB_5 (see the inset in Fig. 5), which indicated that mechanical milling with $AB_{3.5}$ alloy was better than mechanical milling with AB_5 alloy in decreasing the charge-transfer resistance.

Fig. 6 illustrates cyclic voltammograms of the ball-milled AB_2, AB_2–AB_5 and AB_2–$AB_{3.5}$ alloy electrodes at the 50% DOD at 303 K. It was shown that for each alloy sample, the oxidation peak appeared at the potential of around −500 mV (versus Hg/HgO). However, in the investigated potential range the reduction peak did not appear, which might be due to the rapid and hardly detective hydrogen absorption during charge process as reported in Ref. [16]. The previous study [17] showed that the oxidation peak corresponded to the hydrogen desorption from the interior to the surface of the alloy particles, the height of

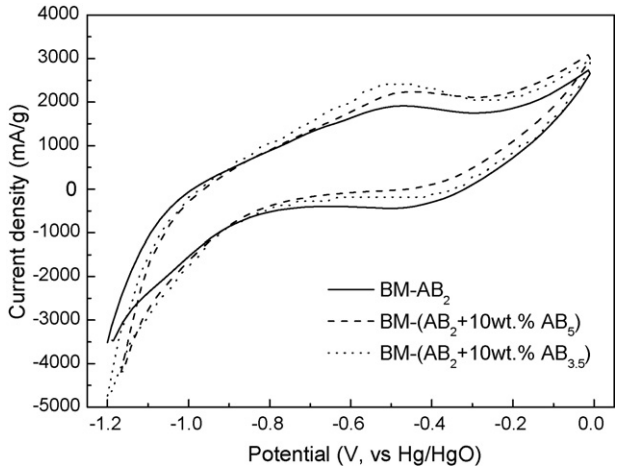

Fig. 6. Cyclic voltammograms of the ball-milled AB_2, AB_2–AB_5 and AB_2–$AB_{3.5}$ composite electrodes at 50% DOD at 303 K.

the oxidation peak reflected the kinetics of the alloy electrodes and the peak area indicated the capacity of hydrogen desorption. In addition, the oxidation current density was mainly influenced by the hydrogen release from the interior of the alloy powder to the surface. As seen from Fig. 6, the height and area of oxidation peak increased to a certain extent after mechanical milling AB_2 alloy with rare-earth alloy AB_5 and $AB_{3.5}$, which indicated that the electrochemical kinetics and the discharge capacity had been improved. Moreover, it was also found that the effect of $AB_{3.5}$ alloy on improving the discharge capacity and the reaction kinetics was better than that of AB_5 alloy. This result was in good agreement with that obtained from the maximum discharge capacity and EIS measurements.

Fig. 7 shows the anodic polarization curves of the ball-milled AB_2, AB_2–AB_5 and AB_2–$AB_{3.5}$ alloy electrodes at the 50% DOD and 303 K. It can be seen that, for all the anodic polarization curves, the anodic current density increased first with increasing overpotential and finally reached a maximum defined as the limiting current density I_L. The limiting current density I_L indicated that an oxidation reaction took place on the surface of the negative electrode and the general oxidation product prevented further penetration of the hydrogen atoms [18]. In addition, the limiting current density I_L was mainly controlled by the hydrogen diffusion in the bulk of alloys [19] and partly influenced by the resistance of the alloy surface. It is generally accepted that the larger the limiting current density I_L value, the faster is the diffusion of the hydrogen atoms in the alloys. The limiting current densities obtained from anodic polarization curves are shown in Table 2. The limiting current density I_L was 889.6 mA/g, 1423.0 mA/g and 1412.2 mA/g for AB_2, AB_2–AB_5 and AB_2–$AB_{3.5}$ alloy electrode, respectively. The variation of the I_L values indicated that the hydrogen diffusivity in the alloy electrodes increased after mechanical milling with rare-earth alloys. Moreover, the effect of AB_5 alloy on improving the behavior of hydrogen diffusion was better than that of $AB_{3.5}$ alloy.

Table 2
The limiting current density and the hydrogen diffusion coefficient of the ball-milled AB_2, AB_2–AB_5 and AB_2–$AB_{3.5}$ composite electrodes

Samples	I_L (mA/g)	a[a] (nm)	D ($\times 10^{-14}$ cm^2/s)
BM-AB_2	889.6	266	0.62
BM-(AB_2–AB_5)	1423.0	252	3.19
BM-(AB_2–$AB_{3.5}$)	1412.2	248	2.35

[a] The average particle radius of samples after mechanical milling treatment.

Fig. 8 shows the semilogarithmic curves of the anodic current versus time responses of the ball-milled AB_2, AB_2–AB_5 and AB_2–$AB_{3.5}$ alloy electrodes. According to the model proposed by Nishina at al. [20], the current responses can be distinguished in two regions. The first one is the shorter time region in which the current decreases rapidly, and the other is the longer time region in which the current decreases slowly in a linear fashion. In this case, hydrogen was supplied from the bulk of the alloy, which was proportional to the concentration gradient of hydrogen atoms with time. The diffusion coefficient of the hydrogen atoms in the bulk of the alloy could be estimated through the slope of the linear region of the corresponding plots according

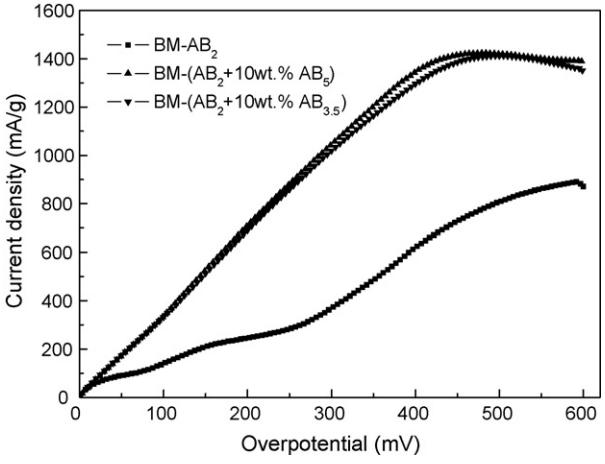

Fig. 7. Anodic polarization curves of the ball-milled AB_2, AB_2–AB_5 and AB_2–$AB_{3.5}$ composite electrodes at 50% DOD at 303 K.

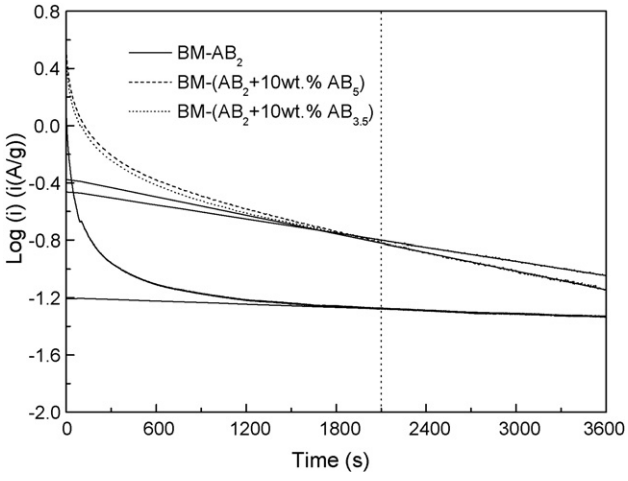

Fig. 8. Semilogarithmic curves of anodic current vs. time response of the ball-milled AB_2, AB_2–AB_5 and AB_2–$AB_{3.5}$ composite electrodes at 303 K.

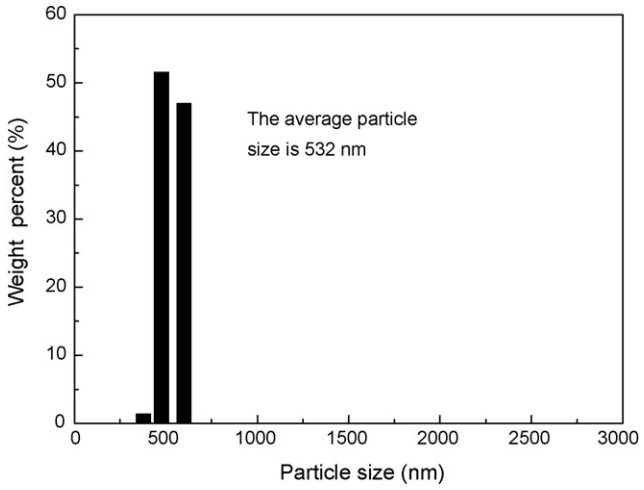

Fig. 9. The particle size distribution of the $Ti_{0.9}Zr_{0.2}Mn_{1.5}Cr_{0.3}V_{0.3}$ alloy after ball milling for 2 h.

to the following expression [21]:

$$\log i = \log\left(\frac{6FD}{da^2}(C_0 - C_s)\right) - \frac{\pi^2}{2.303}\frac{D}{a^2}t \quad (1)$$

where i (A/g) is the diffusion current density, D (cm^2/s) the hydrogen diffusion coefficient, C_0 (mol/cm^3) the initial hydrogen concentration in the bulk of the alloy, C_s (mol/cm^3) the hydrogen concentration on the surface of the alloy particles, a (cm) the alloy particle radius, d (g/cm^3) the density of the hydrogen storage alloy and t (s) is the discharge time. From the particle size measurement as mentioned in Section 2, Fig. 9 shows that the average particle radius of $Ti_{0.9}Zr_{0.2}Mn_{1.5}Cr_{0.3}V_{0.3}$ alloy is 266 nm after mechanical milling treatment for 2 h. According to our careful experiments, the particle size of the alloy after the addition of La–Mg-based alloy is almost the same as that of the sample without the La–Mg-based additive (see Table 2). The hydrogen diffusion coefficient D values calculated by Eq. (1) are summarized in Table 2. It was found that the hydrogen diffusion coefficient D increased about one order of magnitude after mechanical milling with La-based alloys in which the maximum of the hydrogen diffusion coefficient D reached 3.19×10^{-14} cm^2/s for the ball-milled AB_2–AB_5 alloy electrode. This result was consistent with that of anodic polarization curves in Fig. 7. It can be suggested that the additional La-based alloy particles with better electrochemical hydrogen storage capacity provide hydrogen diffusion pathways in the present composite electrode as mentioned above, which is helpful to improve both the hydrogen reaction kinetics and the discharge capacity.

4. Conclusions

In order to improve the electrochemical characteristic of AB_2 Laves phase alloy, AB_2–10 wt.% AB_5 and AB_2–10 wt.% $AB_{3.5}$ composite samples were prepared by mechanical milling $Ti_{0.9}Zr_{0.2}Mn_{1.5}Cr_{0.3}V_{0.3}$ with small amount of rare-earth-based AB_5-type $LaNi_{3.8}Mn_{0.3}Al_{0.4}Co_{0.5}$ alloy and $AB_{3.5}$-type $La_{0.7}Mg_{0.25}Zr_{0.05}Ni_{2.975}Co_{0.525}$ alloy, respectively. X-ray diffraction analysis showed that the addition of rare-earth-based alloys did not change the basic hexagonal C14 Laves phase structure of the original AB_2 alloy. SEM images and EDS patterns indicated that rare-earth alloy particles adhered to the bulk of AB_2 alloy. Compared with ball-milled AB_2 Laves phase alloy, the dramatically improved electrochemical discharge capacity was obtained after mechanical milling AB_2 with rare-earth-based alloys, which amounted to 310.4 mAh/g and 314.0 mAh/g for AB_2–10 wt.% AB_5 and AB_2–10 wt.% $AB_{3.5}$, respectively. However, the cycle life of these composite electrodes needed to be further investigations. The results of EIS and CV indicated that the mechanical milling with $AB_{3.5}$-type $La_{0.7}Mg_{0.25}Zr_{0.05}Ni_{2.975}Co_{0.525}$ alloy helped to decrease the charge-transfer resistance at the electrode surface. However, mechanical milling with AB_5-type $LaNi_{3.8}Mn_{0.3}Al_{0.4}Co_{0.5}$ alloy was beneficial to improving the hydrogen diffusion behavior in the bulk of the composites.

Acknowledgements

This work was financially supported by the National Natural Science Foundation of China (nos. 50671098, 20473091 and 20573112).

References

[1] Y.H. Xu, C.P. Chen, W.X. Geng, Q.D. Wang, Int. J. Hydrogen Energy 26 (2002) 593–596.
[2] Y.Q. Qiao, M.S. Zhao, M.Y. Li, X.J. Zhu, G.Y. Cao, Scripta Mater. 55 (2006) 279–282.
[3] Y.F. Zhu, R. Li, M.X. Gao, Y.F. Liu, H.G. Pan, Q.D. Wang, Trans. Nonferrous Met. Soc. China 13 (2003) 33–37.
[4] Y. Moriwaki, T. Gamo, H. Seri, T. Iwaki, J. Less-Common Met. 172 (1991) 1211–1218.
[5] C. Iwakura, I. Kim, N. Matsui, H. Inoue, M. Matsuoka, Electrochim. Acta 40 (1995) 560–566.
[6] M. Au, F. Pourarian, S. Simizu, S.G. Sankar, L. Zhang, J. Alloys Compd. 223 (1995) 1–5.
[7] L. Zaluski, A. Zaluska, J.O. Ström-Olsen, J. Alloys Compd. 217 (1995) 245–249.
[8] X.B. Yu, G.S. Walker, D.M. Grant, Z. Wu, B.J. Xia, Appl. Phys. Lett. 87 (2005) 133121–133123.
[9] X.B. Yu, T. Dou, Z. Wu, B.J. Xia, J. Shen, Nanotechnology 17 (2006) 268–271.
[10] T.Z. Si, Q.A. Zhang, J. Alloys Compd. 414 (2006) 317–321.
[11] Z.H. Chen, Z.H. Chen, K.L. Huang, P.Y. Huang, J. Alloys Compd. 293-295 (1999) 712–715.
[12] H.G. Pan, Y.F. Liu, M.X. Gao, Y.Q. Lei, Q.D. Wang, J. Electrochem. Soc. 150 (2003) A565–A570.
[13] Y.F. Liu, H.G. Pan, M.X. Gao, Y.F. Zhu, H.W. Ge, S.Q. Li, Y.Q. Lei, Acta Metall. Sin. 39 (2003) 666–672.
[14] H.H. Lee, K.Y. Lee, J.Y. Lee, J. Alloys Compd. 253/254 (1997) 601–604.
[15] N. Kuriyama, T. Sakai, H. Miyamura, I. Uehara, H. Ishikawa, T. Iwasaki, J. Electrochem. Soc. 139 (1992) L72–L73.
[16] S.A. Cheng, Y.Q. Lei, H. Liu, Q.D. Wang, J.Q. Zhang, C.N. Cao, J. Appl. Electrochem. 27 (1997) 1307–1309.
[17] Y.F. Liu, H.G. Pan, M.X. Gao, R. Li, Y.Q. Lei, J. Alloys Compd. 376 (2004) 304–313.
[18] H. Niu, D.O. Northwood, Int. J. Hydrogen Energy 27 (2002) 69–77.
[19] B.V. Ratnakumar, C. Witham, R.C. Bowman, A. Hightower, B. Fultz, J. Electrochem. Soc. 143 (1996) 2578–2584.
[20] T. Nishina, H. Ura, I. Uchida, J. Electrochem. Soc. 144 (1997) 1273–1277.
[21] G. Zheng, B.N. Popov, R.E. White, J. Electrochem. Soc. 142 (1995) 2695–2698.